Am J Physiol Cell Physiol 317: C701–C713, 2019.
First published July 10, 2019; doi:10.1152/ajpcell.00098.2019.

RESEARCH ARTICLE

Uremic metabolites impair skeletal muscle mitochondrial energetics through disruption of the electron transport system and matrix dehydrogenase activity

Trace Thome,[1] Zachary R. Salyers,[1] Ravi A. Kumar,[1] Dongwoo Hahn,[1] Fabian N. Berru,[1] Leonardo F. Ferreira,[1,2] Salvatore T. Scali,[3] and Terence E. Ryan[1,2]

[1]*Department of Applied Physiology and Kinesiology, University of Florida, Gainesville, Florida;* [2]*Center for Exercise Science, University of Florida, Gainesville, Florida; and* [3]*Division of Vascular Surgery and Endovascular Therapy, University of Florida, Gainesville, Florida*

Submitted 22 March 2019; accepted in final form 7 July 2019

Thome T, Salyers ZR, Kumar RA, Hahn D, Berru FN, Ferreira LF, Scali ST, Ryan TE. Uremic metabolites impair skeletal muscle mitochondrial energetics through disruption of the electron transport system and matrix dehydrogenase activity. *Am J Physiol Cell Physiol* 317: C701–C713, 2019. First published July 10, 2019; doi:10.1152/ajpcell.00098.2019.—Chronic kidney disease (CKD) leads to increased skeletal muscle fatigue, weakness, and atrophy. Previous work has implicated mitochondria within the skeletal muscle as a mediator of muscle dysfunction in CKD; however, the mechanisms underlying mitochondrial dysfunction in CKD are not entirely known. The purpose of this study was to define the impact of uremic metabolites on mitochondrial energetics. Skeletal muscle mitochondria were isolated from C57BL/6N mice and exposed to vehicle (DMSO) or varying concentrations of uremic metabolites: indoxyl sulfate, indole-3-acetic-acid, L-kynurenine, and kynurenic acid. A comprehensive mitochondrial phenotyping platform that included assessments of mitochondrial oxidative phosphorylation (OXPHOS) conductance and respiratory capacity, hydrogen peroxide production (JH_2O_2), matrix dehydrogenase activity, electron transport system enzyme activity, and ATP synthase activity was employed. Uremic metabolite exposure resulted in a ~25–40% decrease in OXPHOS conductance across multiple substrate conditions ($P < 0.05$, $n = 5–6$/condition), as well as decreased ADP-stimulated and uncoupled respiratory capacity. ATP synthase activity was not impacted by uremic metabolites; however, a screen of matrix dehydrogenases indicated that malate and glutamate dehydrogenases were impaired by some, but not all, uremic metabolites. Assessments of electron transport system enzymes indicated that uremic metabolites significantly impair complex III and IV. Uremic metabolites resulted in increased JH_2O_2 under glutamate/malate, pyruvate/malate, and succinate conditions across multiple levels of energy demand (all $P < 0.05$, $n = 4$/group). Disruption of mitochondrial OXPHOS was confirmed by decreased respiratory capacity and elevated superoxide production in cultured myotubes. These findings provide direct evidence that uremic metabolites negatively impact skeletal muscle mitochondrial energetics, resulting in decreased energy transfer, impaired complex III and IV enzyme activity, and elevated oxidant production.

bioenergetics; chronic kidney disease; mitochondria; skeletal muscle; uremia

INTRODUCTION

Chronic kidney disease (CKD) is defined as any condition that causes reduced kidney function and affects more than 25 million Americans (18, 24). CKD patients often present with debilitating myopathic symptoms including muscle weakness, fatigue, and muscle wasting, which negatively impact functional independence and quality of life leading to increased morbidity and mortality (2, 44). Previous work in rodent and human studies has implicated the activation of proteolytic pathways such as the ubiquitin proteasome system, caspase-3, calpains, and the dysregulation of autophagy resulting in increased protein catabolism and muscle wasting (7, 27, 38, 39, 44, 49, 50). Several studies have also associated systemic inflammation and/or muscle fibrosis to muscle dysfunction in CKD (1, 7, 43, 48). Despite this body of literature, the molecular mechanism(s) by which impaired kidney function leads to activations of these pathways in skeletal muscle is not known.

Interestingly, the cellular pathways linked to muscle wasting in CKD have all been shown to be stimulated by reactive oxygen species (ROS) (11, 17, 30, 32). Given that mitochondria are a major site of ROS production, it has been suggested that mitochondria may play a pivotal role in the development of skeletal muscle dysfunction in CKD. To this end, it was recently reported that human CKD patients exhibit lower mitochondrial ATP/O_2 ratio (measured in vivo with magnetic resonance and optical spectroscopy), a measure of mitochondrial efficiency (33). Rodent studies have also reported altered mitochondrial morphology, elevated markers of oxidative stress, and decreased mitochondrial content, as well as decreased ATP production and mitochondrial respiration (3, 31, 38, 46). Despite this growing evidence, the underlying biological mechanism by which CKD negatively impacts mitochondrial energetics is poorly understood.

A major function of the kidneys is to rid the body of waste materials that are either ingested or produced endogenously by normal metabolism. However, CKD results in retention of these waste products, termed uremia (8, 10, 40, 41). In fact, one of these uremic metabolites, indoxyl sulfate, has recently garnered attention, as it was shown to induce morphological and functional changes in skeletal muscle mitochondria resulting in muscle atrophy (10, 37). In these studies, exposure of cultured muscle cells to indoxyl sulfate resulted in decreased cellular respiratory capacity and elevated ROS production. Although these recent studies demonstrate a role of indoxyl

Address for reprint requests and other correspondence: T. E. Ryan, Dept. of Applied Physiology and Kinesiology, Univ. of Florida, 1864 Stadium Rd., Gainesville, FL 32611 (e-mail: ryant@ufl.edu).

sulfate, the molecular mechanisms through which indoxyl sulfate disrupted mitochondrial metabolism is still unknown. Moreover, CKD results in the accumulation of ~100 uremic metabolites (41) which potentially negatively impact skeletal muscle. Interestingly, some of the metabolites that accumulate are protein bound and poorly filtered by modern dialysis membranes (29, 41). Thus, uremic toxicity of skeletal muscle remains a concern even for patients receiving hemodialysis. Interestingly, some of the most concentrated uremic metabolites found in the blood of CKD patients are derived from intestinal tryptophan metabolism through indolic and kynurenine pathways, including indoxyl sulfate, indole 3-acetic acid, kynurenine, and kynurenic acid (8, 23, 29, 40, 41).

In this study, we aimed to establish the impact of selected uremic metabolites on skeletal muscle mitochondrial energetics based on the hypothesis that uremic metabolites would disrupt mitochondrial metabolism. To accomplish this goal, a comprehensive assessment of mitochondrial energy transfer involving measurements of oxidative phosphorylation (OXPHOS) conductance, hydrogen peroxide emission, dehydrogenase activity, and ATP synthase activity performed in skeletal muscle mitochondria exposed to varying concentrations of uremic metabolites was employed. This platform allows for the investigation of both the global and site-specific impact of uremic metabolites on oxidative metabolism. Acute exposure to uremic metabolites resulted in decreased mitochondrial conductance through oxidative phosphorylation and subsequently increased hydrogen peroxide production. Additional enzymatic assays demonstrated that uremic metabolites impair some matrix dehydrogenases and directly reduce maximal activity of mitochondrial complexes III and IV but have no impact ATP synthase activity. Uremia-induced impairments in mitochondrial metabolism were confirmed with intact muscle cell cultures. Taken together, these findings provide the first evidence of a molecular mechanism underlying the development of skeletal muscle mitochondrial impairments in CKD.

METHODS

Chemicals and reagents. All chemicals and reagents were obtained from Millipore-Sigma, Research Products International, Combi blocks, and GIBCO (ThermoScientific). A complete list of all suppliers/catalog numbers for reagents used in these studies is available in Table 1. Uremic metabolites tested were dissolved in DMSO at equal concentrations such that equivalent volumes were added for each experiment.

Animals. Ten-week-old male C57BL/6N mice were obtained from Taconic Biosciences ($n = 26$). All mice were housed in a temperature- (22°C) and light-controlled (12:12-h light-dark) room and maintained on standard chow with free access to food and water. All mice were euthanized between 8:00 and 9:00 AM eastern standard time for mitochondrial isolations. All animal experiments adhered to the *Guide for the Care and Use of Laboratory Animals* from the Institute for Laboratory Animal Research, National Research Council, Washington, D.C., National Academy Press, 1996, and any updates. All procedures were approved by the Institutional Animal Care and Use Committee of the University of Florida.

Preparation of isolated skeletal muscle mitochondria. Skeletal muscle mitochondria were isolated as previously described (34, 35). Briefly, skeletal muscle was dissected from mice and placed in mitochondrial isolation medium (300 mM sucrose, 10 mM HEPES, and 1 mM EGTA, pH 7.1). Dissected muscle was then trimmed and cleaned to remove connective tissue or fat. The muscle was minced on ice, placed in ice-cold mitochondrial isolation medium with bovine serum albumin (BSA, 1 mg/mL), homogenized on ice using a glass-Teflon homogenizer (Wheaton), and subsequently centrifuged at 800 *g* to pellet nonmitochondrial myofibrillar proteins, nuclei, and other cellular components. The resulting supernatant was collected and centrifuged at 10,000 *g* to pellet mitochondria. All steps were performed at 4°C. The mitochondrial pellet was gently resuspended in mitochondrial isolation medium (without BSA), and protein concentration was determined by calculation of a standard curve with an albumin standard (ThermoScientific cat. no. SL256970). All mitochondrial isolations used for functional experiments had less than a 15% increase in pyruvate/malate/ADP-supported respiration with the addition of exogenous cytochrome *c* to ensure high integrity of the outer mitochondrial membrane.

Measurement of OXPHOS conductance. High-resolution respirometry was measured using Oroboros Oxygraph-2k (O2K) measuring oxygen flux (J_{O_2}) at 37°C in *buffer Z* (105 mM K-MES, 30 mM KCl, 1 mM EGTA, 10 mM K_2HPO_4, 5 mM $MgCl_2$-$6H_2O$, 2.5 mg/mL BSA, pH 7.1), supplemented with 5 mM creatine (Cr). In this assay, a creatine kinase (CK) clamp was employed to leverage the enzymatic activity of CK, which couples the interconversion of ATP and ADP to that of phosphocreatine (PCr) and free creatine, to titrate the extra mitochondrial ATP/ADP ratio; thus, free energy of ATP hydrolysis (ΔG_{ATPe}) was calculated from the added phosphocreatine (PCr)/creatine (Cr) ratio as done previously (12, 15, 16), where R is the gas constant (8.3145 J/kmol) and T is temperature in kelvin (310.15).

$$\Delta G_{ATPe} = \Delta G_{ATP} + RT \ln\left[(Cr)(P_i)/(PCr)(k_{ck})\right]$$

This approach permits assessment of mitochondrial flux across a range of ATP free energy states which is set experimentally by altering the Cr/PCr ratio (Fig. 1, *A–C*). Overall, the ΔG_{ATP} can be plotted against the corresponding J_{O_2}, creating a linear force-flow relationship, where the slope represents the conductance throughout the electron transport system (ETS) as shown in Fig. 1*B*. In this assay, the ΔG_{ATP} is manipulated through titrations of PCr, which results in a corresponding reduction in ADP concentrations (Fig. 1*C*). 25 μg of mitochondria were added to the O2K chamber in 2 mL of *buffer Z* supplemented with ATP (5 mM), Cr (5 mM), PCr (1 mM), and CK (20 U/mL) and incubated with uremic toxins (indoxyl sulfate, indole-3-acetic acid, kynurenic acid, and L-kynurenine) at specific concentrations (100 nM, 10 μM, 100 μM, and 1 mM) or vehicle (DMSO) for 10 min. All assessments were done at 37°C. Conductance measurements were performed under the following conditions: pyruvate (5 mM) + malate (2.5 mM), glutamate (10 mM) + malate (2.5 mM), and succinate (10 mM) + rotenone (0.005 mM).

Classical measurement of mitochondrial respiratory capacity. In addition to experiments using the creatine kinase energetic clamp, classical respiration assays were performed using high-resolution respirometry (Oroboros Oxygraph) to measure J_{O_2} at 37°C in *buffer Z* (105 mM K-MES, 30 mM KCl, 1 mM EGTA, 10 mM K_2HPO_4, 5 mM $MgCl_2$-$6H_2O$, 2.5 mg/mL BSA, pH 7.1), supplemented with 20 mM creatine. For these experiments, the oxygraph was loaded with assay buffer followed by 10 μM of the desired uremic metabolite and 25 μg of mitochondria. Three substrate conditions were tested: pyruvate (5 mM) + malate (2.5 mM), glutamate (10 mM) + malate (2.5 mM), and succinate (10 mM) + rotenone (0.005 mM). The assays were initiated by the addition of substrates followed by 4 mM ADP, 10 μM cytochrome *c*, and 1 μM carbonyl cyanide 4-(trifluoromethoxy)phenylhydrazone (FCCP).

ATP synthase activity. To assess ATP synthase activity, the ATP synthase needs to be isolated from the rest of the ETS, where in the absence of a proton gradient it will function to hydrolyze ATP and form ADP (ATP→ADP), as previously described (6, 12). Isolated mitochondria were incubated with Cell lytic M (Sigma C2978) at 2 mg/mL to lyse mitochondria. *Buffer E* [HEPES (20 mM), KCl (100 mM), KH_2PO_4 (2.5 mM), $MgCl_2$-$6H_2O$ (2.5 mM), and 1% glycerol] was supplemented with lactate dehydrogenase (10 mM), pyruvate kinase (10 mM), rotenone (0.005 mM), phosphoenol-pyruvate (PEP,

Table 1. *Complete list of chemicals and reagents utilized*

Item Description	Cat. No.	Supplier
α-Ketoglutaric acid	K1750	Millipore-Sigma
Adenosine 5′-diphosphate (ADP)	A5285	Millipore-Sigma
Alamethicin from *Trichoderma viride*	A4665	Millipore-Sigma
Amplex Ultra Red (AUR)	A36006	Millipore-Sigma
Antimycin A (AMA)	A8674	Millipore-Sigma
Auranofin	A6733	Millipore-Sigma
β-Nicotinamide adenine dinucleotide hydrate (NADH)	N1636	Millipore-Sigma
β-Nicotinamide adenine dinucleotide salt (NAD+)	N0632	Millipore-Sigma
Boric acid	B6768	Millipore-Sigma
Bovine serum albumin (BSA)	A7030	Millipore-Sigma
Calcein acetoxymethyl ester	206700	Millipore-Sigma
Cell lytic M	C2978	Millipore-Sigma
Creatine kinase	C3755	Millipore-Sigma
Creatine monohydrate	C3630	Millipore-Sigma
Coenzyme A trilithium salt	C3019	Millipore-Sigma
Cytochrome *c* from equine heart	C2506	Millipore-Sigma
D-Glucose	G32030	Research Products International
Decylubiquinone (DCU)	D7911	Millipore-Sigma
2,6-Dichloroindophenol sodium salt hydrate (DCPIP)	D1878	Millipore-Sigma
Dimethyl sulfoxide (DMSO)	276855	Millipore-Sigma
n-Dodecyl β-D-maltoside	D4641	Millipore-Sigma
Dulbecco's modified Eagle's medium	10569	ThermoScientific
EDTA	E57045	Research Products International
EGTA	E57060	Research Products International
Ethidium homodimer-1 (EtHD-1)	46043	Millipore-Sigma
FCCP (carbonyl cyanide-*p*-phenyl-hydrazone)	C2920	Millipore-Sigma
Fetal bovine serum (FBS)	97068	VWR
L-Glutamic acid	G5889	Millipore-Sigma
Glycerol	G22025	Research Products International
HEPES	H3375	Millipore-Sigma
Hanks' balanced salt solution (HBSS)	24020	ThermoScientific
Horseradish peroxidase (HRP)	P8375	Millipore-Sigma
Horse serum	26050	ThermoScientific
Hydrogen peroxide, 30%	H325–100	ThermoScientific
Indole-3-acetic acid sodium salt	I5148	Millipore-Sigma
Indoxyl sulfate potassium salt	I3875	Millipore-Sigma
Insulin/transferrin/selenium	41400	ThermoScientific
Invitrogen Molecular Probes MitoSOX Red Mitochondrial Superoxide Indicator	M36008	ThermoScientific
Kynurenic acid	K3375	Millipore-Sigma
L-Kynurenine	K8625	Millipore-Sigma
Lactate dehydrogenase/pyruvate kinase	P0294	Millipore-Sigma
Magnesium chloride kexahydrate	M24000	Research Products International
Malic acid	M7397	Millipore-Sigma
Malonate	M1296	Millipore-Sigma
MES potassium salt	M0895	Millipore-Sigma
3-Methyl-2-oxopentanoic acid sodium salt	198978	Millipore-Sigma
Myxothiazol	T5580	Millipore-Sigma
Oligomycin A	75351	Millipore-Sigma
Pierce BCA protein assay kit	PI23225	ThermoScientific
Penicilin-streptomycin	15140	ThermoScientific
Phosphoenol-pyruvate (PEP)	10108294001	Millipore-Sigma
Potassium chloride (KCl)	P9541	Millipore-Sigma
Potassium cyanide (KCN)	60178	Millipore-Sigma
Potassium phosphate (K_2HPO_4) dibasic	P3786	Millipore-Sigma
Potassium phosphate (KH_2PO_4) monobasic	P2670	Millipore-Sigma
Potassium pyruvate	QA1116	Combi-Blocks
Rotenone	R8875	Millipore-Sigma
Sodium borohydride	452882	Millipore-Sigma
Succinic acid	S42000	Research Products International
Sucrose	S24060	Research Products International
Superoxide dismutase from bovine erythrocytes	S7446	Millipore-Sigma
Thiamine pyrophosphate (TPP)	C8754	Millipore-Sigma
Tris-adenosine triphosphate (ATP)	A9062	Millipore-Sigma
Tris-phosphocreatine (PCr)	P1937	Millipore-Sigma
Triton X-100	X100	Millipore-Sigma
Trypsin-EDTA (0.25%)	252000	ThermoScientific

5 mM), and NADH (0.2 mM). NADH levels were determined via autofluorescence [excitation/emission (Ex/Em): 340/450 nm]. Specific concentrations of uremic toxins (100 nM, 100 μM, and 1 mM), 2 μg of isolated mitochondria, and 200 μL of assay buffer were added to a 96-well plate. All reactions were performed at 37°C in a BioTek Synergy 2 Multimode Microplate Reader. For this assay, the ATP synthase functions to hydrolyze ATP, because lysis of the mitochondria will dissipate their ability to establish a membrane potential (which normally drives ATP synthesis). Using a pyruvate kinase/lactate dehydrogenase-coupled assay, ATP hydrolysis by the ATP synthase was coupled to NADH consumption in a 1:1 stoichiometry (Fig. 3*A*). Thus, the rate of decrease in NADH autofluorescence can be used as a measure of maximal ATP synthase activity. Fluorescence values were converted to picomoles of NADH via an NADH standard curve.

Matrix dehydrogenase activity. The activity of several mitochondrial matrix dehydrogenases (*J*NADH) was measured fluorometrically using NADH autofluorescence (Ex/Em = 340/450 nm) in a 96-well plate read kinetically on a BioTek Synergy 2 Multimode Microplate Reader. For all assays, *buffer Z* was supplemented with alamethicin (0.03 mg/mL), rotenone (0.005 mM), and NAD+ (2 mM). For pyruvate dehydrogenase, α-ketoglutarate dehydrogenase, and branched-chain ketoacid dehydrogenase, the assay buffer was supplemented with cofactors coenzyme A (0.1 mM), and thiamine pyrophosphate (0.3 mM). For each dehydrogenase, assay buffer was loaded, followed by mitochondria and 0.5 mM of the desired uremic metabolite. Mitochondria were allowed to permeabilize and incubate with the uremic metabolic for 10 min. Dehydrogenase activity was then initiated by addition of the following substrates run in parallel: pyruvate (5 mM), malate (5 mM), glutamate (10 mM), α-ketoglutarate (10 mM), or α-keto-β-methylvalerate (5 mM). Rates of NADH production were calculated as the slope of linear portions of the NADH curves. Fluorescence values were converted to picomoles of NADH via an NADH standard curve.

Assessment of mitochondrial OXPHOS complex activity. Enzyme activity of all electron transport system (ETS) complexes were determined spectrophotometrically as previously described (6, 36), with slight modification described below. Isolated mitochondria were diluted to 0.5 mg/mL in Cell Lytic M (Millipore-Sigma) or hypotonic buffer (25 mM K_2HPO_4, 5.3 mM MgCl, pH 7.2) and subjected to three freeze-thaw cycles before use. Mitochondrial lysates were incubated with uremic metabolites at 0.5 mM in their respective assay buffers for 10 min before the reactions were initiated. Complex I activity was determined in 50 mM potassium phosphate, 3 mg/mL BSA, 240 μM KCN, 0.4 μM antimycin A, 50 μM decyl-ubiquinone, and 80 μM 2,6-dichlorophenolindophenol (DCPIP). NADH oxidation (0.8 mM) was measured through reduction of DCPIP at 600 nm. All complex I activity measurements were corrected for rotenone-insensitive NADH oxidation following the addition of 25 μM rotenone, and rates were converted to moles using an extinction coefficient of 19,100 $M^{-1}cm^{-1}$. Complex II (succinate dehydrogenase, SDH) activity was assessed in the following assay buffer: 10 mM KH_2PO_4, 2 mM EDTA, and 1 mg/mL BSA at pH 7.8. Briefly, the assay buffer was supplemented with 0.004 mM rotenone, 0.2 mM ATP, 10 mM succinate, and 0.08 mM DCPIP. Mitochondria were preincubated with 0.2 mM succinate for 30 min at room temperature, and then 5 μg/well was added to a 96-well plate containing 200 μL of assay buffer and 0.5 mM of the desired uremic metabolite. Following a 10-min incubation at 37°C, the assay was initiated by addition of oxidized decyl-ubiquinone (0.08 mM), and reduction of DCPIP followed at 600 nm. Rates were converted to moles using the extinction coefficient of 19,100 $M^{-1}cm^{-1}$. As a negative control, malonate was included to inhibit SDH. Complex III activity was measured in 10 mM KH_2PO_4, 2 mM EDTA, and 1 mg/mL BSA at pH 7.8 supplemented with 0.2 mM ATP, 0.24 mM KCN, and 0.04 mM oxidized cytochrome *c*. Complex III activity was determined kinetically by measuring the reduction of cytochrome *c* following the addition of reduced decyl-ubiquinone (0.15 mM) at 550 nm, and rates were converted to moles using an extinction coefficient of 18,500 $M^{-1}cm^{-1}$. Specificity of the assay was confirmed by the absence of cytochrome *c* reduction in the presence of myxothiazol (10 μM). Complex IV activity was measured in 10 mM KH_2PO_4, 250 mM sucrose, and 1 mg/mL BSA at pH 6.5 supplemented with 2.5 mM maltoside and 5 μM antimycin A following the addition of 110 μM reduced cytochrome *c* by following the decrease in absorbance at 550 nm. Potassium cyanide (625 μM) was used to confirm the specificity of complex IV activity.

H_2O_2 production. Mitochondrial H_2O_2 production was measured fluorometrically via an Amplex Ultra Red (AUR)/horseradish peroxidase (HRP) detection system (Ex: Em 530:590), as described previously (12, 13, 35). H_2O_2 production was measured in *buffer Z* supplemented with Cr (5 mM), CK (20 U/mL) AUR (10 μM), HRP (1 U/mL), superoxide dismutase (SOD, 20 U/mL), ATP (5 mM), and auranofin (0.1 μM). Using the the creatine kinase clamp, experiments were run using three levels of energy demand set by the addition of PCr at 6, 15, or 30 mM. H_2O_2 production was assessed with the following substrate conditions: pyruvate (5 mM) + malate (2.5 mM), glutamate (5 mM) + malate (2.5 mM), and succinate (10 mM). All reactions were done at 37°C, 200 μL of volume, and 5–20 μg of mitochondria in the BioTek Synergy 2 Multimode Microplate Reader. Rates were collected and converted to picomoles H_2O_2·per minute per milligram using a standard curve. Auranofin was added to inhibit the endogenous thioredoxin buffering system within the mitochondrial matrix, therefore allowing a more accurate approximation of total H_2O_2 produced under respiratory conditions (12). Fluorescence values were converted to picomoles of H_2O_2 via a H_2O_2 standard curve.

Cell culture. Immortalized murine C_2C_{12} myoblasts were purchased from ATCC (CRL-1772). Myoblasts were grown to ~90% confluence in Dulbecco's modified Eagle's medium (DMEM) + GlutaMAX (GIBCO cat. no. 10569) supplemented with 10% fetal bovine serum (FBS; VWR cat. no. 97068), and 1% penicillin-streptomycin (GIBCO cat. no. 15140) at standard culture conditions (37°C in 5% CO_2). Once cells had reached 90% confluence, myotube differentiation was initiated via serum withdrawal by placing cells in differentiation medium [DMEM supplemented with 2% horse serum (GIBCO cat. no. 26050), 1% penicillin-streptomycin, and 1% insulin-transferrin-selenium (GIBCO cat. no. 41400)]. Differentiation medium was changed every 24 h for 6 days to form mature myotubes.

Measurement of cell viability. Mature myotubes were treated with 0.5 mM DMSO (control), indoxyl sulfate, indole-3-acetic acid, L-kynurenine, or kynurenic acid for 18 h in differentiation medium at 37°C in 5% CO_2. Following uremic metabolite treatment, myotubes were rinsed with warm PBS and incubated with 10 μM ethidium homodimer-1 (EtHD-1; Millipore-Sigma cat. no. 46043) in warm Hanks' balanced salt solution (HBSS, GIBCO cat. no. 24020) for 15 min at 37°C in 5% CO_2. After the 15-min incubation, HBSS and Et-HD-1 were aspirated, and fresh HBSS was added to the plate for imaging with an Evos FL2 Auto inverted fluorescent microscope (ThermoScientific). EtHD-1 is a cell-impermeant viability indicator that is strongly fluorescent when bound to DNA. Myotubes treated with 0.25% Triton X-100 in HBSS to permeabilize cell membranes were used as a positive control. EtHD-1-positive nuclei were quantified and expressed as a percentage of the Triton X-100-treated control cells by using custom batch processing routines in Cell Profiler (The Broad Institute). Cell viability was further confirmed by staining live cells with 1 μM calcein acetoxymethyl ester.

Measurement of myotube respiratory function. Mature myotubes were incubated with the specified uremic metabolites (indoxyl sulfate, indole-3-acetic acid, kynurenic acid, and L-kynurenine) or vehicle (DMSO) for 18 h at 37°C in 5% CO_2. After 18 h of uremic metabolite exposure, cells were rinsed with PBS, trypsinized with 0.25% trypsin-EDTA (GIBCO cat. no. 25200) and centrifuged at 800 *g* for 5 min to pellet myotubes. Myotubes were resuspended in 2.5 mL of *buffer Z* supplemented with glucose (10 mM) and pyruvate (5 mM). Cells were loaded into the Oxygraph O2K chamber (Oroboros), and respiration

was measured at 37°C. Basal oxygen consumption (JO_2) was measured in intact myotubes followed by sequential additions of oligomycin A (1 μg/μL) to examine ATP-linked respiration, a titration of carbonyl cyanide 4-(trifluoromethoxy)phenylhydrazone FCCP (250 nM to 1.5 μM) to determine maximal respiratory capacity, followed by the addition of rotenone (0.01 mM) and antimycin A (0.005 mM) to determine nonmitochondrial oxygen consumption. Rates of oxygen consumption were normalized to protein content measured by BCA assay (ThermoScientific) and expressed as picomoles per milligram per second.

Measurement of myotube superoxide production. Mature myotubes were treated with uremic metabolites for 18 h before staining with MitoSOX (ThermoScientific cat. no. M36008), a fluorogenic probe used to approximate mitochondrial-derived superoxide. After 18 h of treatment, myotubes were washed twice with HBSS and incubated with 500 nM MitoSOX for 15 min in HBSS before imaging. Sixteen ×20 images were captured per sample (n = 4–5 samples per group) and analyzed using custom-written routines in CellProfiler (The Broad Institute) to assess both MitoSOX-positive area and mean intensity. All processing procedures were performed uniformly over the entire set of images by using batch processing modes to remove any human input.

Statistical analysis. Data are presented as means ± SD. Comparisons of data with more than two groups were performed using

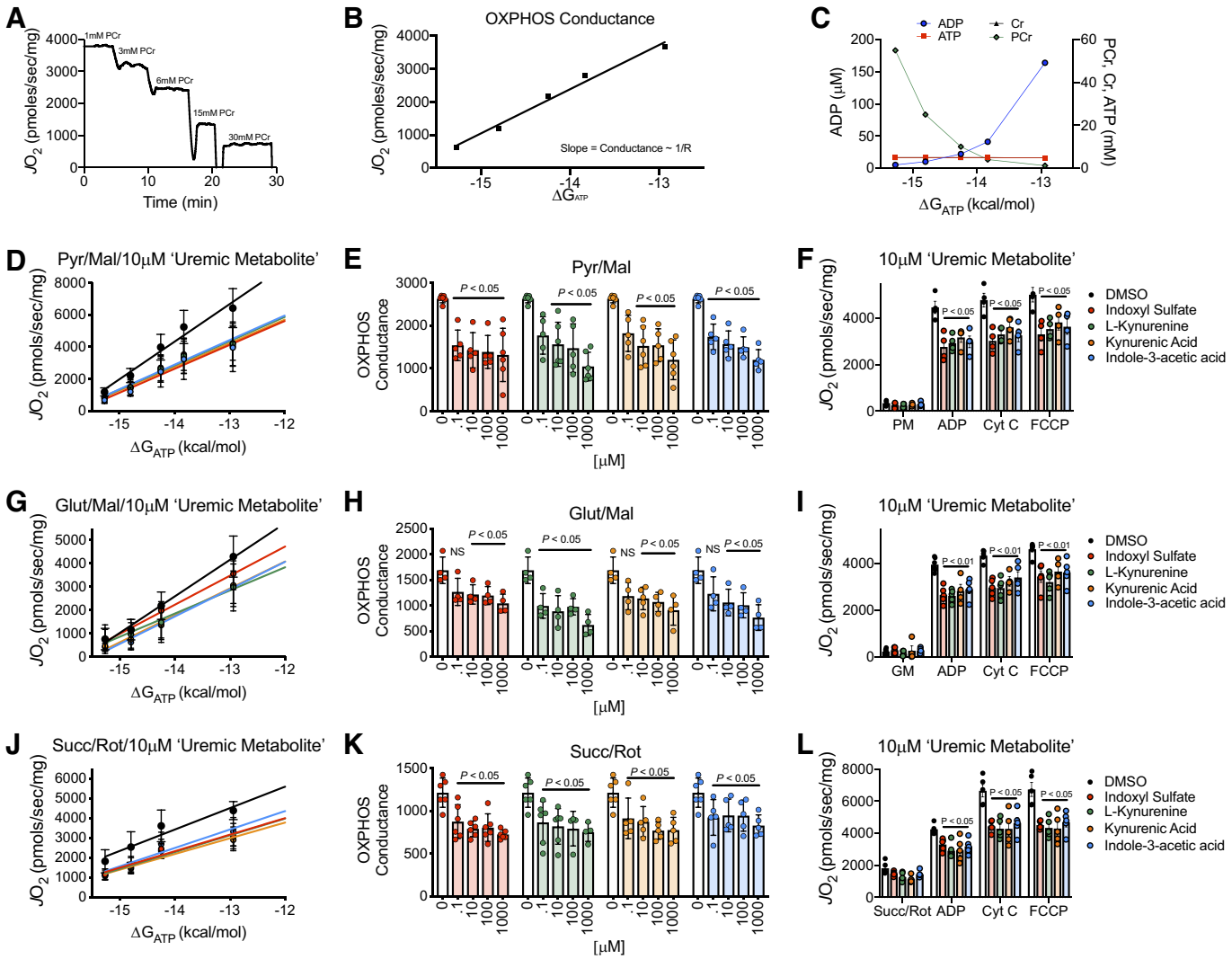

Fig. 1. Uremic metabolites decrease mitochondrial oxidative phosphorylation (OXPHOS) conductance and respiratory capacity. Skeletal muscle mitochondria were isolated from C57BL/6N mice. *A*: mitochondrial OXPHOS was assessed using a creatine kinase (CK) clamp system, by which mitochondrial respiration (JO_2) is altered by sequential additions of phosphocreatine (PCr) in a buffer containing creatine, ATP, and excess creatine kinase. Through the creatine kinase equilibrium, this assay allows for direct calculation of extracellular energy demand (ΔG_{ATP}), such that mitochondria are assessed at varying levels of energy demand. *B*: conductance through the OXPHOS system is calculated from the linear relationship (i.e., slope) between JO_2 and ΔG_{ATP}. *C*: calculated concentrations of ATP, ADP, PCr, and Cr across the range of energy demands examined in conductance assays. *D*: plot of JO_2 and ΔG_{ATP} supported by pyruvate and malate following acute (10 min) incubation with 10 μM of uremic metabolites. *E*: quantification of OXPHOS conductance across a range of uremic metabolite concentrations supported by pyruvate/malate (PM). CytC, cytochrome *c*. *F*: maximal ADP-stimulated and uncoupled (FCCP) respiratory capacity supported by pyruvate and malate. *G*: plot of JO_2 and ΔG_{ATP} supported by glutamate and malate following acute (10 min) incubation with 10 μM of uremic metabolites. *H*: quantification of OXPHOS conductance across a range of uremic metabolite concentrations supported by glutamate/malate. *I*: maximal ADP-stimulated and uncoupled (FCCP) respiratory capacity supported by glutamate and malate (GM). *J*: plot of JO_2 and ΔG_{ATP} supported by succinate and rotenone following acute (10 min) incubation with 10 μM of uremic metabolites. *K*: quantification of OXPHOS conductance across a range of uremic metabolite concentrations supported by succinate+rotenone. *L*: maximal ADP-stimulated and uncoupled (FCCP) respiratory capacity supported by succinate and rotenone; n = 4–6 biologically independent mitochondrial preparations per condition.

two-way ANOVA with Tukey's post hoc testing for comparisons between control (DMSO) and each uremic metabolite-treated sample. We did not perform statistical comparisons between uremic metabolites but instead compared each to the DMSO-treated control group with a two-way ANOVA with Tukey's post hoc testing. All statistical analysis was performed in GraphPad Prism (version 7.0). In all cases, $P < 0.05$ was considered statistically significant.

RESULTS

Uremic metabolites decrease OXPHOS conductance and respiratory capacity. To examine the impact of uremic metabolites on mitochondrial energetics, a physiological assessment of OXPHOS conductance was performed. This experiment involved the addition of extracellular creatine kinase, excess creatine monohydrate, and ATP, followed by additions of phosphocreatine, which through the CK reaction established the extracellular energy charge (ΔG_{ATP}) and thus the energy demand. The mitochondrial system responds to changes in the ΔG_{ATP} by rapidly adjusting mitochondrial ATP synthesis (and, thus, oxygen consumption; see Fig. 1*A*). Plotting the mitochondrial respiratory flux as a function of ΔG_{ATP} allows for the calculation of conductance (i.e., slope of the relationship) or resistance within the ETS using Ohm's law ($I = V/R$). A greater slope indicates higher conductance (or less resistive force) within the mitochondrial energy system (Fig. 1*B*).

Acute (10 min) incubation with uremic metabolites (indoxyl sulfate, indole-3-acetic acid, L-kynurenine, and kynurenic acid), resulted in significant decreases in OXPHOS conductance when mitochondria were energized with pyruvate-malate (Fig. 1, *D* and *E*) or glutamate-malate (Fig. 1, *G* and *H*), as well as succinate-rotenone (Fig. 1, *J* and *K*). Indolic metabolites (indoxyl sulfate and indole-3-acetic acid) decreased OXPHOS conductance ~30–50% across a range of concentrations from 100 nM to 1 mM, whereas kynurenine pathway metabolites (L-kynurenine and kynurenic acid) decreased OXPHOS conductance by ~10–15% at 100 nM and ~50–60% at 1 mM concentrations. These findings indicate that the presence of uremic metabolites, even at low concentrations, impair the mitochondria's ability to respond to changes in energy demand, a process that is crucial for optimal performance in skeletal muscle. In addition to the energetic clamp experiments, mitochondrial respiratory capacity was also assessed using classical bolus ADP-type experiments where mitochondria were energized with substrate followed by the addition of saturating (4 mM) ADP. Acute incubation (10 min) with all uremic metabolites resulted in a significant decrease in maximal ADP-supported respiration with pyruvate-malate (Fig. 1*F*), glutamate-malate (Fig. 1*I*), and succinate-rotenone (Fig. 1*L*). Respiratory rates following the addition of FCCP, which uncouples oxygen consumption from ATP synthesis, were also significantly deceased in the presence of all uremic metabolites, suggesting the impact of uremic metabolites is upstream of the ATP synthase. Notably, decreased OXPHOS conductance and mitochondrial respiratory capacity were observed at concentrations of uremic metabolites that were near or much lower than those reported in plasma from CKD patients [indoxyl sulfate, 500 μM; indole-3-acetic acid, 64 μM; L-kynurenine, 15 μM; kynurenic acid, 5 μM; concentrations estimated based on an adult blood volume of 4.7 liters, from the following references (8, 40)].

Uremic metabolites do not alter ATP synthase activity. Within the OXPHOS system, there are several sites where increased resistance (or decreased conductance) can originate. These include the following: *1*) the generation of redox charge (i.e., $NADH/NAD^+$ and $FADH_2/FAD^+$) through catabolism of fuel by matrix dehydrogenases, *2*) the electron transport system, which transfers the potential energy from the redox charge into an electrochemical proton gradient, and *3*) the ATP synthase, which drives the synthesis of ATP through consumption of the proton motive force. Thus, based on the observation of decreased OXPHOS conductance in the presence of uremic metabolites, additional experiments were designed to determine which of these sites were negatively impacted by uremic metabolites.

The observation that uncoupled mitochondrial respiratory capacity was decreased in the presence of uremic metabolites suggests that these metabolites exert their effects upstream of the ATP synthase. To more directly assess the ATP synthase, we used an enzyme-coupled assay (6, 12) in which ATP hydrolysis by the ATP synthase enzyme (the natural reaction of

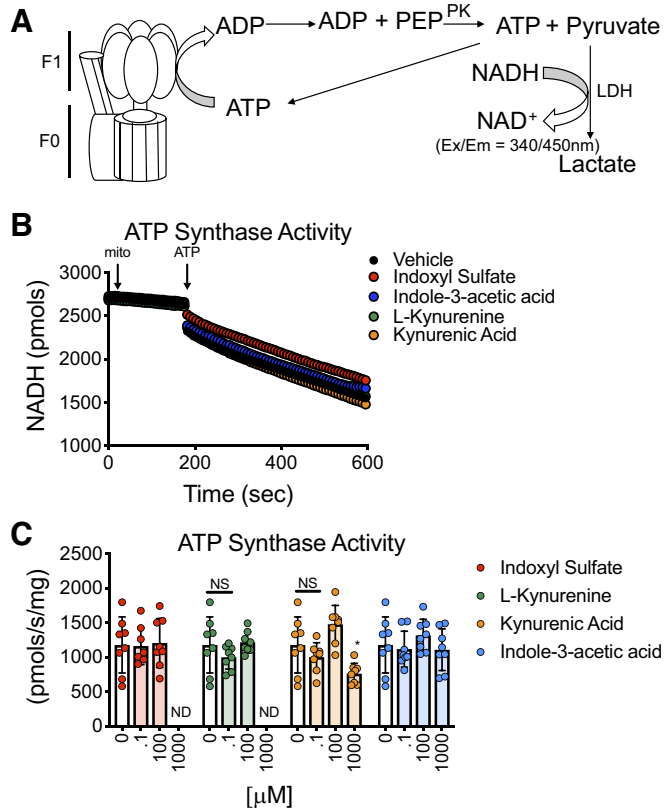

Fig. 2. Uremic metabolites do not alter ATP synthase activity. Mitochondria were lysed to determine whether uremic metabolites impacted the ATP synthase enzyme. *A*: graphic depiction of the enzyme-coupled assay employed. In the absence of the proton motive force, ATP synthase will function to hydrolyze ATP into ADP, which was linked to pyruvate kinase (PK) and lactate dehydrogenase (LDH) to allow for measurement of NADH consumption that occurs 1:1 with ATP hydrolysis. PEP, phosphoenol-pyruvate. *B*: representative NADH curves for mitochondria treated with 100 μM uremic metabolites. *C*: quantification of ATP synthase activity across a range of concentrations of uremic metabolites. Note: ATP synthase activity could not be obtained at 1 mM concentrations of indoxyl sulfate and L-kynurenine due to disruption of NADH standard curves at this concentration; $n = 8$ biologically independent mitochondrial preparations per condition. $^*P < 0.05$ vs. control (DMSO treated). ND, not detected.

the ATP synthase in the absence of a proton motive force) is coupled to NADH consumption through the addition of exogenous pyruvate kinase and lactate dehydrogenase and their respective substrates (Fig. 2*A*). A representative trace of ATP synthase activity assays in the presence of uremic metabolites (100 μM) is shown in Fig. 2*B*. Quantification of ATP synthase activity assays indicated that, similarly to PDH, uremic metabolites did not disrupt ATP synthase activity, with the exception being 1 mM concentrations of kynurenic acid (Fig. 2*C*). However, it is worth noting that a decrease in OXPHOS conductance was observed in all uremic metabolites, including kynurenic acid, at concentrations below the millimolar range. Taken together, these findings demonstrate that the decreased OXPHOS conductance caused by uremic metabolites is not mediated by impairment of the ATP synthase and/or ADP/ATP transport.

Uremic metabolites selectively impair matrix dehydrogenase and mitochondrial ETS enzyme activity. Next, experiments were performed to examine the impact of uremic metabolites on multiple matrix dehydrogenases, which are responsible for generation of the redox charge (NADH/NAD). To this end, mitochondria were permeabilized with alamethicin, and dehydrogenase activity (J_{NADH}) was assessed at saturating substrate concentrations. Interestingly, the uremic metabolites tested displayed unique interactions with various dehydrogenases. Pyruvate and branched-chain ketoacid dehydrogenases were unaffected by all metabolites even at 0.5 mM concentrations (Fig. 3, *A* and *B*). In contrast, malate (MDH), glutamate (GDH), and α-ketoglutarate dehydrogenase (AKGDH) all displayed sensitivity to some, but not all, uremic metabolites. MDH was substantially inhibited by indoxyl sulfate, kynurenic acid, and L-kynurenine, but not indole-3-acetic acid (Fig. 3*C*). GDH was inhibited only by kynurenic acid (Fig. 3*D*), and AKGDH was inhibited by both kynurenic acid and L-kynurenine (Fig. 3*E*).

To explore whether uremic metabolites have direct interactions with mitochondrial electron transport proteins, biochemical assays assessing the maximal activity of mitochondrial

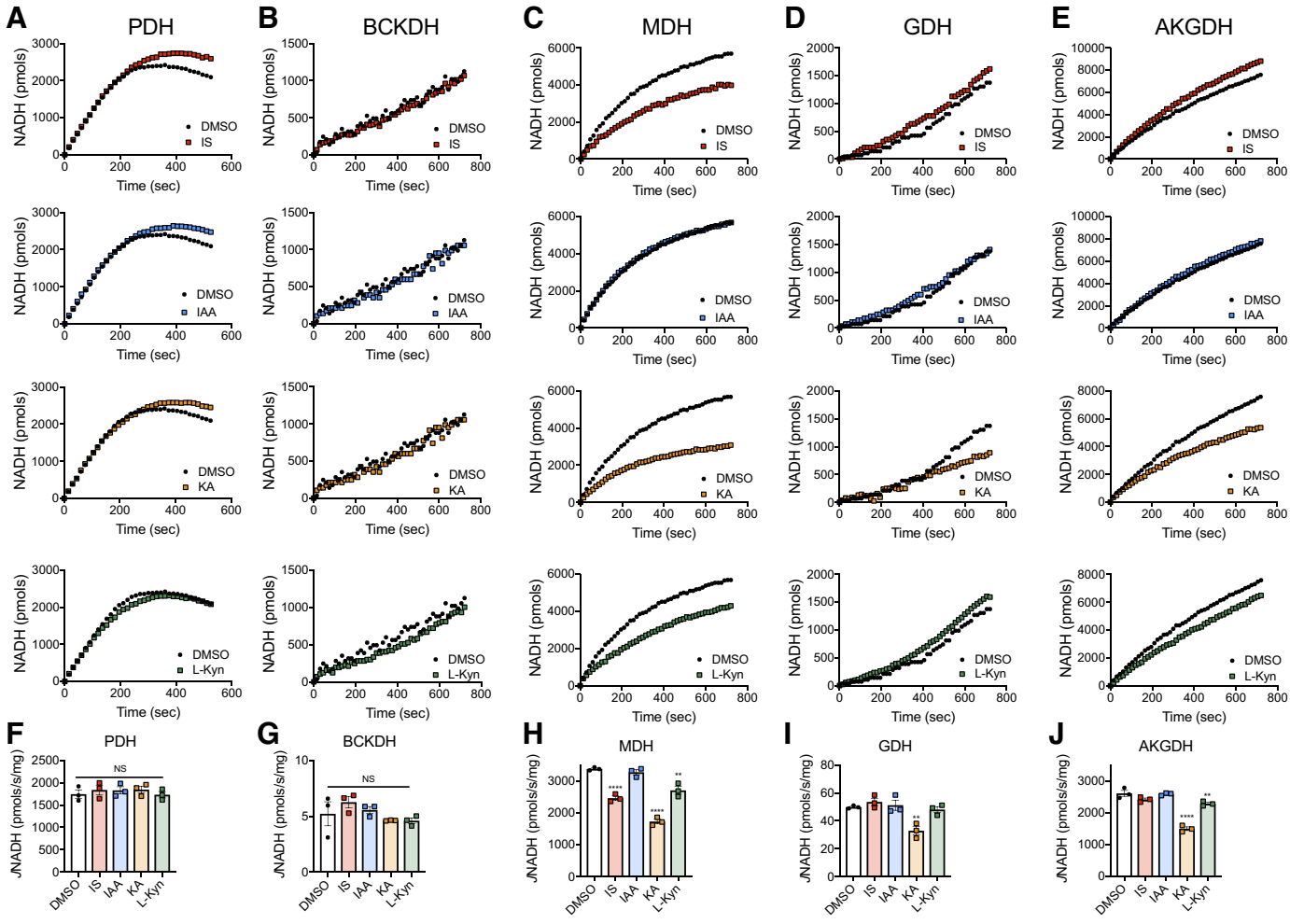

Fig. 3. Uremic metabolites selectively impact matrix dehydrogenase activity. To determine whether uremic metabolites altered matrix dehydrogenase activity, a screen of NADH-generating dehydrogenases was performed. To accomplish this, mitochondria were permeabilized with alamethicin and provided saturating substrate in the presence of rotenone (to inhibit NADH oxidation by complex I). NAD^+ reduction was measured kinetically using autofluorescence with excitation/emission at 340/450 nm. Each uremic metabolite was screened at 0.5 mM following a 10-min incubation. Representative enzyme assays are shown for pyruvate dehydrogenase (PDH; *A*), branched-chain ketoacid dehydrogenase (BCKDH; *B*), malate dehydrogenase (MDH; *C*), glutamate hydrogenase (GDH; *D*), and α-ketoglutarate dehydrogenase (AKGDH; *E*). Quantification of NADH production from PDH (*F*), BCKDH (*G*), MDH (*H*), GDH (*I*), and AKGDH (*J*). $^{**}P < 0.01$, $^{****}P < 0.0001$ vs. DMSO-treated control; $n = 3$ biologically independent mitochondrial preparations per condition. NS, not significant; IS, indoxyl sulfate; IAA, indole-3-acetic acid; KA, kynurenic acid; L-Kyn, L-kynurenine.

complexes I–IV were performed in the presence or absence of uremic metabolites. Interestingly, complex I (NADH dehydrogenase) and complex II (succinate dehydrogenase) were not impacted by the presence of any uremic metabolites (0.5 mM; Fig. 4, *A* and *B*). However, complex III (ubiquinol-cytochrome *c* oxidoreductase) activity was lower in the presence of all uremic metabolites (Fig. 4*C*) and complex IV (cytochrome-*c* oxidase) activity was impaired by indoxyl sulfate, kynurenic acid, and L-kynurenine, but not indole-3-acetic acid (Fig. 4*D*). The discovery that uremic metabolites impact enzyme activity downstream of the quinone cycle is supported by the findings of decreased OXPHOS conductance and respiratory capacity under both complex I-linked substrates (pyruvate-malate and glutamate-malate) as well as complex II-linked substrates (succinate).

Uremic metabolites disrupt the ETS and potentiate electron leak. Based on the principles of bioenergetics, a decrease in respiratory conductance (or increased resistance) would promote electron leak and thus elevate mitochondrial-derived oxidative stress. To this end, measurements of hydrogen peroxide production ($J_{H_2O_2}$) in isolated mitochondria energized by pyruvate-malate, glutamate-malate, or succinate were performed under conditions where the extracellular energy demand was set through the extracellular CK system. Consistent with the principles of bioenergetics, the presence of uremic metabolites increased $J_{H_2O_2}$ in all substrate conditions across three levels of energy demand for all uremic metabolites tested (Fig. 5). In most cases, rates of hydrogen peroxide production increased as the concentration of uremic metabolites was increased. These data provide further evidence that uremic metabolites disrupt the mitochondrial ETS, leading to impaired oxygen consumption and elevated ROS production.

With the current data, accurate calculations of mitochondrial electron leak ($J_{H_2O_2}/J_{O_2}$) are not possible for a few reasons: *1*) hydrogen peroxide production assays were performed in the presence of auranofin (a thioredoxin reductase inhibitor), whereas respiratory conductance assays were not; and *2*) respiratory conductance assays for succinate included rotenone (to prevent reverse electron flow), whereas hydrogen peroxide emission did not include rotenone. Nonetheless, it is important to consider that exposure of mitochondria to uremic metabolites decreased respiration (mainly at higher levels of energy demand) and elevated peroxide production. These combined events likely resulted from substantial increases in electron leak. Crude estimations of electron leak at near-resting levels of energy demand ($\Delta G_{ATP} = -15.23$ kcal/mol) suggest that electron leak increased 2- to 3-fold with pyruvate-malate and 1.3-fold with glutamate-malate in the presence of uremic metabolites.

Uremic metabolites disrupt mitochondrial energetics in intact myotubes. Because isolation procedures could alter the functional/physiological properties of the mitochondria (28), additional experiments were undertaken to examine mitochondrial energetics in cultured, intact, mature myotubes. First, assessments of cell viability were performed in differentiated C_2C_{12} myotubes that were exposed to uremic metabolites (0.5 mM) to confirm that uremic metabolite treatment was not inducing cell death. Indeed, high-dose exposure to uremic metabolites did not induce muscle cell death (Fig. 6*A*), measured by assessing cell permeability through staining with ethidium homodimer-1 (a non-cell-permeable fluorescent probe that binds DNA). Next, mature myotubes were treated with uremic metabolites for 18 h before measurement of cellular respiratory function. Consistent with the findings in isolated mitochondria, uremic metabolite exposure (both 10 and 100 μM) decreased maximal respiratory capacity in myotubes by 13–50% (Fig. 6*B*). To further verify a disruption within the ETS system which was observed in isolated mitochondria exposed to the uremic metabolites, mature myotubes were incubated with the uremic metabolites for 18 h and assessed for oxidative stress through MitoSOX. MitoSOX is a fluorescent probe that reacts with mitochon-

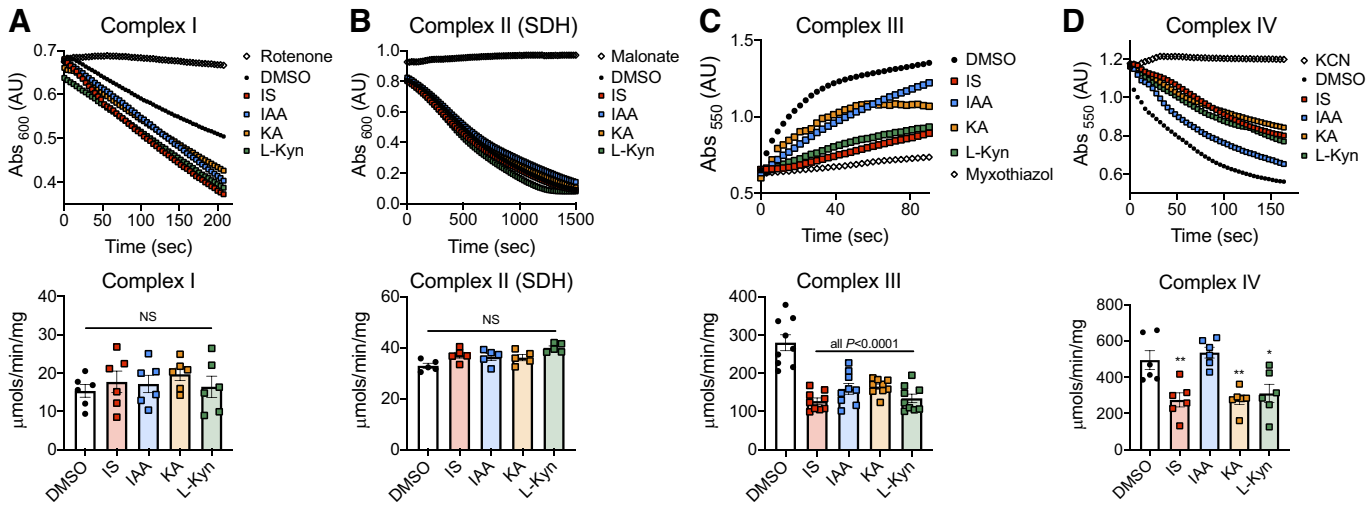

Fig. 4. Uremic metabolites impair mitochondrial complex III and IV enzyme activities. The impact of uremic metabolites on mitochondrial electron transport system enzymes was assessed using standard biochemical assays. *A*: representative kinetic traces and quantification of maximal enzyme activity for complex I (NADH dehydrogenase). *B*: representative kinetic traces and quantification of maximal enzyme activity for complex II (succinate dehydrogenase). *C*: Rrepresentative kinetic traces and quantification of maximal enzyme activity for complex III (ubiquinol-cytochrome *c* oxidoreductase). *D*: representative kinetic traces and quantification of maximal enzyme activity for complex IV (cytochrome-*c* oxidase). $^*P < 0.05$, $^{**}P < 0.01$ vs. DMSO-treated control. $N = 5$–9 biologically independent mitochondrial preparations per condition. NS, not significant; IS, indoxyl sulfate; IAA, indole-3-acetic acid; KA, kynurenic acid; L-Kyn, L-kynurenine; KCN, potassium cyanide.

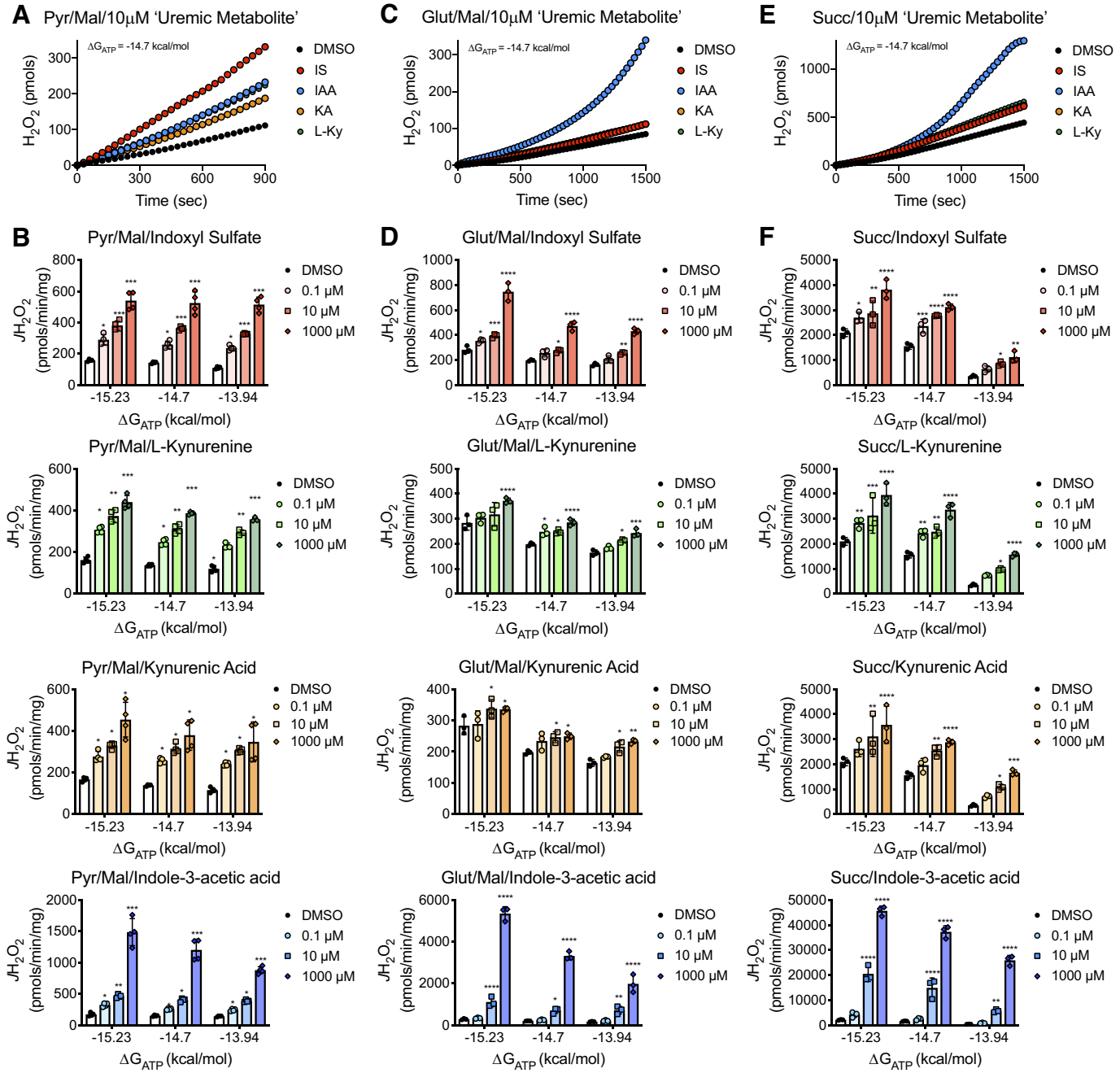

Fig. 5. Uremic metabolites increase mitochondrial H_2O_2 production. Mitochondrial H_2O_2 production was assessed using AmplexUltraRed assay in the presence of the creatine kinase clamp system, which allows for assessments across several levels of energy demand. *A*: representative H_2O_2 production traces for mitochondria energized with pyruvate/malate. *B*: quantification of H_2O_2 production rates under pyruvate/malate conditions at 3 levels of energy demand. *C*: representative H_2O_2 production traces for mitochondria energized with glutamate/malate. *D*: quantification of H_2O_2 production rates under glutamate/malate conditions at 3 levels of energy demand. *E*: representative H_2O_2 production traces for mitochondria energized with succinate. *F*: quantification of H_2O_2 production rates under succinate conditions at 3 levels of energy demand. $^*P < 0.05$, $^{**}P < 0.01$, $^{***}P < 0.001$, $^{****}P < 0.0001$ vs. control (DMSO treated); $n = 3$–4 biologically independent mitochondrial isolations.

drial-derived superoxide radical, allowing us to quantify radical production. Exposure of C_2C_{12} myotubes to uremic metabolites increased MitoSOX-positive area and mean intensity by ~25% (all $P < 0.0001$ vs. DMSO-treated control cells) compared with the vehicle control (Fig. 6, *C*–*E*). This increase in oxidative stress was comparable to that of myotubes treated with antimycin A, an inhibitor of complex III in the mitochondria. All together, these data confirm that uremic metabolites disrupt mitochondrial energetics in an intact muscle cell system, confirming observations made in isolated mitochondria.

DISCUSSION

Chronic kidney disease (CKD) leads to progressive debilitating symptoms, including muscle weakness, fatigue, and muscle wasting, that contribute to increased morbidity and

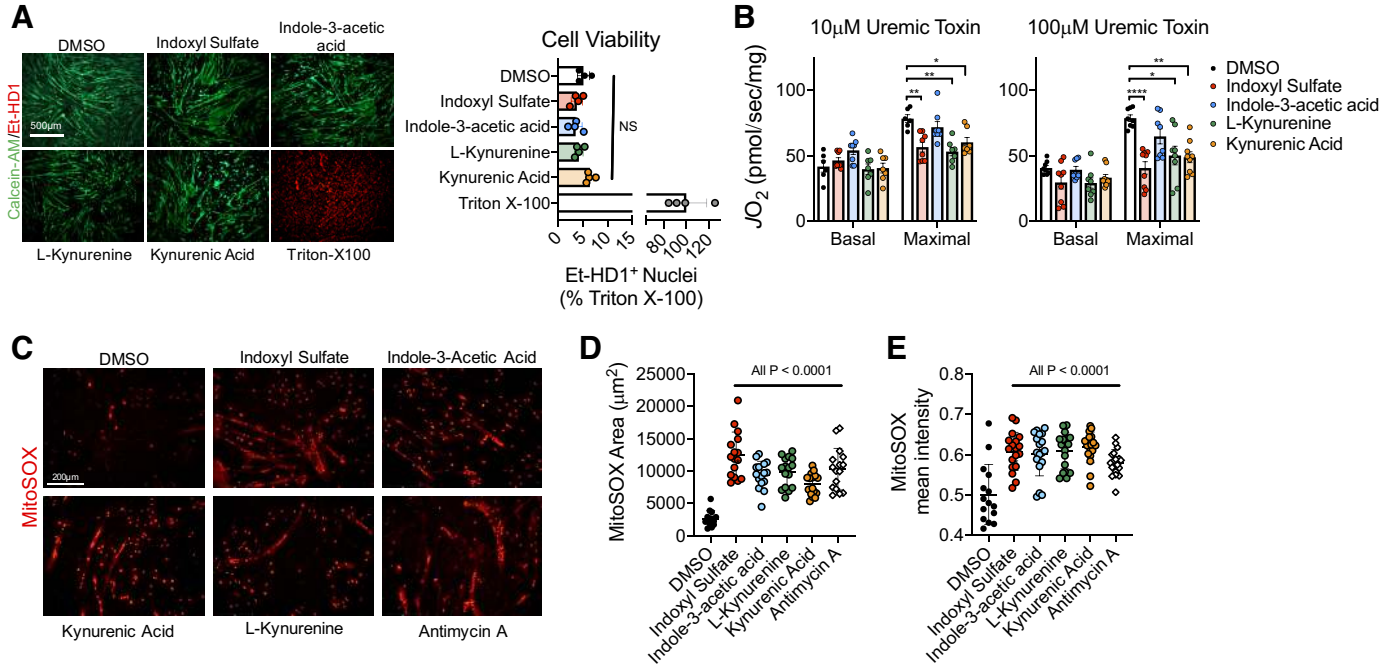

Fig. 6. Uremic metabolites disrupt mitochondrial energetics in intact, cultured myotubes. Mature C_2C_{12} myotubes were exposed to uremic metabolites for 18 h. *A*: uremic metabolite treatment at 100 μM did not alter cell viability [cells stained positive for ethidium homodimer-1 (EtHD-1)]. *B*: maximal respiratory capacity was significantly lower in myotubes treated with uremic metabolites at 10 and 100 μM. *C*: mitochondrial superoxide production was assessed by MitoSOX staining of mature myotubes. Consistent with isolated mitochondria, intact myotubes treated with 100 μM of uremic metabolites increased both mitoSOX-positive area (*D*) and mean mitoSOX intensity (*E*), indicating greater mitochondrial-derived oxidative stress. Antimycin A treatment (complex III inhibitor, 25 nM) was used as a positive control for MitoSOX experiments; $n = 4–8$/condition for viability and respirometry; $n = 15–18$/group for MitoSOX analysis. $^*P < 0.05$, $^{**}P < 0.01$, $^{****}P < 0.0001$ vs. control (DMSO treated). NS, not significant.

mortality in these patients (19, 20, 39, 44). Previous evidence suggests that impaired mitochondrial function may be a primary cause for muscle impairment in CKD (3, 14, 31, 33, 38, 44, 46, 47). Using muscle biopsies from CKD patients (stage 5 on hemodialysis), one group reported lower mitochondrial volume and mtDNA copy number compared with healthy control muscle specimens (14). Another study reported lower mitochondrial ATP/O_2 ratios, a measure of mitochondrial efficiency (with magnetic resonance and optical spectroscopy), in skeletal muscle of CKD patients (33). Several additional studies have also reported altered muscle mitochondrial morphology, protein expression, and reduced mitochondrial respiratory function in rodents and humans with CKD (3, 46, 50). However, despite these reported findings, the underlying biological mechanism by which CKD negatively impacts mitochondria is unknown. In this study, a comprehensive assessment of mitochondrial energetics was performed in the presence or absence of known uremic metabolites, which have been shown to accumulate in the blood of CKD patients (40). This diagnostic platform demonstrated that several uremic metabolites decrease mitochondrial energy transfer through interactions with the mitochondrial ETS complexes III and IV as well as some matrix dehydrogenase (malate, glutamate, and malate, glutamate, and α-ketoglutarate dehydrogenases) that result in decreased enzyme activity. Consequently, disruption of these mitochondrial enzymes resulted in decreased OXPHOS conductance and respiratory capacity and elevated electron leak and, subsequently, superoxide radical formation leading to elevated mitochondrial hydrogen peroxidase production. These observations were confirmed using intact cultures of mature myotubes. Taken together, these findings provide the first evidence of a mechanism by which impaired kidney function leads to mitochondrial impairments in skeletal muscle via uremic metabolite accumulation.

Previous research on the mechanisms of muscle dysfunction in CKD has primarily focused on activation of proteolytic, autophagic, and atrophy pathways [comprehensively reviewed by Wang and Mitch (44)]. Using rodent models, investigators have established that CKD results in activation of the ubiquitin-proteasome pathway (22), caspase-3 and associated kinases (27, 45), and autophagy (38, 50), as well as impaired IGF-I signaling (4, 49). Additionally, systemic inflammation and fibrosis have also been associated with the development of muscle dysfunction in CKD (1, 7, 20, 43, 48). Interestingly, these catabolic pathways that lead to muscle atrophy are known to be stimulated by oxidative stress (11, 17, 30). Thus, the discovery that uremic metabolites disrupt the mitochondrial ETS, leading to increased ROS would align with this body of literature. In fact, the disruption of the mitochondrial ETS and resulting oxidative stress may be an upstream signal activating proteolytic, autophagic, and atrophy signaling cascades. Indeed, if this hypothesis is substantiated in future studies, therapeutic development aimed at improving mitochondrial energetics and/or preventing interactions with uremic metabolites may be warranted to improve health outcomes and quality of life for CKD patients.

CKD currently has no cure, and the only treatment options are kidney transplant and dialysis. However, transplant numbers are far outpaced by the increasing prevalence of CKD, whereas hemodialysis aims to filter waste products from the

blood. Unfortunately, a number of uremic solutes/metabolites, including those studied herein, are protein bound and not adequately filtered by dialysis membranes and thus remain in the blood despite dialysis treatment (23, 29). In this study, the uremic metabolites that were examined are believed to be derived from endogenous tryptophan metabolism via the kynurenine and indolic metabolic pathways, which are normally cleared by the kidneys and excreted in the urine. Indeed, the studied metabolites are robustly increased in blood samples obtained from CKD patients (8, 40, 41). Indoxyl sulfate has been the subject of focus in previous work. Specifically, it has been reported that indoxyl sulfate treatment (1 mM) of C_2C_{12} myotubes resulted in myotube atrophy, increased inflammatory signaling, and elevated oxidative stress and myostatin expression (9). These authors went on to deliver indoxyl sulfate to half-nephrectomized mice, a rodent model of CKD. Mice treated with indoxyl sulfate for 12 wk displayed increased myostatin expression and decreased myofiber cross-sectional area compared with control mice (9). Consistent with results from this study, another group recently reported that indoxyl sulfate decreased maximal respiration and increased reactive oxygen species production (hydroxyl radical measured by electron spin resonance) in cultured myotubes (37). The finding that uremic metabolites have negative impacts on cell biology/function has sparked interest in the development of spherical carbon-adsorbent compounds that bind to certain small-molecular-weight organic compounds, such as some uremic metabolites (21, 42). In this regard, a recent study administered AST-120, an oral adsorbent compound, to mice with CKD that resulted in reduced plasma indoxyl sulfate levels, improved exercise capacity and increased mitochondrial citrate synthase activity compared with placebo-treated CKD mice (26).

A challenge for therapeutic development might be the pluripotent effects of uremic metabolites on mitochondrial metabolism. The comprehensive assessments employed herein demonstrated that each uremic metabolite that is elevated in CKD patients may have specific interactions with one or several mitochondrial enzymes/proteins. For example, malate dehydrogenase activity was impaired by indoxyl sulfate, kynurenic acid, and L-kynurenine, whereas glutamate dehydrogenase was significantly impaired only by kynurenic acid. Moreover, kynurenic acid and L-kynurenine decreased α-ketoglutarate dehydrogenases, but not pyruvate or branched-chain ketoacid dehydrogenases, which have similar multienzyme complex structures. It is not clear as to the mechanism underlying this discrepancy, but it may be related to differences in the organization or composition of these large multienzyme complexes. It is important to consider that uremic metabolites were tested individually in the current study; however, CKD patients experience increased concentrations of all tested uremic metabolites as well as several dozen more metabolites that may have unknown effects on mitochondrial metabolism. While the literature on uremic metabolites and skeletal muscle mitochondria is sparse (outside of studies on indoxyl sulfate described above), a few studies have reported negative effects on mitochondria from other tissue/cell types. Indole-3-acetic acid was shown to decrease mitochondrial respiratory capacity in renal proximal tubular epithelial cells (25). Another study reported that kynurenine pathway metabolites 3-hydroxykynurenine and 3-hydroxyanthranilic acid (both downstream of L-kynurenine) impaired cardiac mitochondrial respiratory function (5).

In summary, this study found that uremic metabolites, which are normally filtered by the kidneys but accumulate in CKD patients, disrupt skeletal muscle mitochondrial energetics through interactions with the electron transport system and some matrix dehydrogenases. Consequently, mitochondrial oxidative phosphorylation is substantially impaired, and electron leak is increased, leading to elevated mitochondrial oxidative stress. These findings report the first mechanistic evidence of a direct impact of uremic metabolites on mitochondrial function in skeletal muscle. These observations align with previous studies in rodent and human CKD models demonstrating activation of proteolytic, autophagic, and atrophy pathways, which are known to be redox sensitive. Thus, mitochondrial alterations caused by uremic metabolites could be the initiating cause of the progressive muscle weakness, atrophy, and fatigue that are often reported by CKD patients. Future studies aimed to evaluate the therapeutic potential of targeting skeletal muscle mitochondrial energetics in CKD are warranted.

GRANTS

This work was supported in part by American Heart Association Grant 18CDA34110044 (to T. E. Ryan) and National Heart, Lung, and Blood Institute Grant R01HL130318 (to L. F. Ferreira).

DISCLOSURES

No conflicts of interest, financial or otherwise, are declared by the authors.

AUTHOR CONTRIBUTIONS

T.T., S.T.S., and T.E.R. conceived and designed research; T.T., Z.R.S., R.A.K., D.H., F.N.B., L.F.F., and T.E.R. performed experiments; T.T., Z.R.S., R.A.K., D.H., F.N.B., L.F.F., and T.E.R. analyzed data; T.T., Z.R.S., R.A.K., D.H., F.N.B., L.F.F., S.T.S., and T.E.R. interpreted results of experiments; T.T., Z.R.S., and T.E.R. prepared figures; T.T. and T.E.R. drafted manuscript; T.T., Z.R.S., R.A.K., D.H., F.N.B., L.F.F., S.T.S., and T.E.R. edited and revised manuscript; T.T., Z.R.S., R.A.K., D.H., F.N.B., L.F.F., S.T.S., and T.E.R. approved final version of manuscript.

REFERENCES

1. **Abramowitz MK, Paredes W, Zhang K, Brightwell CR, Newsom JN, Kwon HJ, Custodio M, Buttar RS, Farooq H, Zaidi B, Pai R, Pessin JE, Hawkins M, Fry CS.** Skeletal muscle fibrosis is associated with decreased muscle inflammation and weakness in patients with chronic kidney disease. *Am J Physiol Renal Physiol* 315: F1658–F1669, 2018. doi:10.1152/ajprenal.00314.2018.
2. **Androga L, Sharma D, Amodu A, Abramowitz MK.** Sarcopenia, obesity, and mortality in US adults with and without chronic kidney disease. *Kidney Int Rep* 2: 201–211, 2017. doi:10.1016/j.ekir.2016.10.008.
3. **Avin KG, Chen NX, Organ JM, Zarse C, O'Neill K, Conway RG, Konrad RJ, Bacallao RL, Allen MR, Moe SM.** Skeletal muscle regeneration and oxidative stress are altered in chronic kidney disease. *PLoS One* 11: e0159411, 2016. doi:10.1371/journal.pone.0159411.
4. **Bailey JL, Zheng B, Hu Z, Price SR, Mitch WE.** Chronic kidney disease causes defects in signaling through the insulin receptor substrate/phosphatidylinositol 3-kinase/Akt pathway: implications for muscle atrophy. *J Am Soc Nephrol* 17: 1388–1394, 2006. doi:10.1681/ASN.2004100842.
5. **Baran H, Staniek K, Kepplinger B, Stur J, Draxler M, Nohl H.** Kynurenines and the respiratory parameters on rat heart mitochondria. *Life Sci* 72: 1103–1115, 2003. doi:10.1016/S0024-3205(02)02365-2.
6. **Barrientos A, Fontanesi F, Díaz F.** Evaluation of the mitochondrial respiratory chain and oxidative phosphorylation system using polarography and spectrophotometric enzyme assays. *Curr Protoc Hum Genet* 63: 19.3.1–19.3.14, 2009. doi:10.1002/0471142905.hg1903s63.
7. **Deger SM, Hung AM, Gamboa JL, Siew ED, Ellis CD, Booker C, Sha F, Li H, Bian A, Stewart TG, Zent R, Mitch WE, Abumrad NN, Ikizler TA.** Systemic inflammation is associated with exaggerated skeletal muscle protein catabolism in maintenance hemodialysis patients. *JCI Insight* 2: 95185, 2017. doi:10.1172/jci.insight.95185.

8. **Duranton F, Cohen G, De Smet R, Rodriguez M, Jankowski J, Vanholder R, Argiles A; European Uremic Toxin Work Group.** Normal and pathologic concentrations of uremic toxins. *J Am Soc Nephrol* 23: 1258–1270, 2012. doi:10.1681/ASN.2011121175.
9. **Enoki Y, Watanabe H, Arake R, Fujimura R, Ishiodori K, Imafuku T, Nishida K, Sugimoto R, Nagao S, Miyamura S, Ishima Y, Tanaka M, Matsushita K, Komaba H, Fukagawa M, Otagiri M, Maruyama T.** Potential therapeutic interventions for chronic kidney disease-associated sarcopenia via indoxyl sulfate-induced mitochondrial dysfunction. *J Cachexia Sarcopenia Muscle* 8: 735–747, 2017. doi:10.1002/jcsm.12202.
10. **Enoki Y, Watanabe H, Arake R, Sugimoto R, Imafuku T, Tominaga Y, Ishima Y, Kotani S, Nakajima M, Tanaka M, Matsushita K, Fukagawa M, Otagiri M, Maruyama T.** Indoxyl sulfate potentiates skeletal muscle atrophy by inducing the oxidative stress-mediated expression of myostatin and atrogin-1. *Sci Rep* 6: 32084, 2016. doi:10.1038/srep32084.
11. **Filomeni G, De Zio D, Cecconi F.** Oxidative stress and autophagy: the clash between damage and metabolic needs. *Cell Death Differ* 22: 377–388, 2015. doi:10.1038/cdd.2014.150.
12. **Fisher-Wellman KH, Davidson MT, Narowski TM, Lin CT, Koves TR, Muoio DM.** Mitochondrial diagnostics: a multiplexed assay platform for comprehensive assessment of mitochondrial energy fluxes. *Cell Reports* 24: 3593–3606.e10, 2018. doi:10.1016/j.celrep.2018.08.091.
13. **Fisher-Wellman KH, Lin CT, Ryan TE, Reese LR, Gilliam LA, Cathey BL, Lark DS, Smith CD, Muoio DM, Neufer PD.** Pyruvate dehydrogenase complex and nicotinamide nucleotide transhydrogenase constitute an energy-consuming redox circuit. *Biochem J* 467: 271–280, 2015. doi:10.1042/BJ20141447.
14. **Gamboa JL, Billings FT IV, Bojanowski MT, Gilliam LA, Yu C, Roshanravan B, Roberts LJ II, Himmelfarb J, Ikizler TA, Brown NJ.** Mitochondrial dysfunction and oxidative stress in patients with chronic kidney disease. *Physiol Rep* 4: e12780, 2016. doi:10.14814/phy2.12780.
15. **Glancy B, Barstow T, Willis WT.** Linear relation between time constant of oxygen uptake kinetics, total creatine, and mitochondrial content in vitro. *Am J Physiol Cell Physiol* 294: C79–C87, 2008. doi:10.1152/ajpcell.00138.2007.
16. **Glancy B, Willis WT, Chess DJ, Balaban RS.** Effect of calcium on the oxidative phosphorylation cascade in skeletal muscle mitochondria. *Biochemistry* 52: 2793–2809, 2013. doi:10.1021/bi3015983.
17. **Hyatt H, Deminice R, Yoshihara T, Powers SK.** Mitochondrial dysfunction induces muscle atrophy during prolonged inactivity: a review of the causes and effects. *Arch Biochem Biophys* 662: 49–60, 2019. doi:10.1016/j.abb.2018.11.005.
18. **Jha V, Garcia-Garcia G, Iseki K, Li Z, Naicker S, Plattner B, Saran R, Wang AY, Yang CW.** Chronic kidney disease: global dimension and perspectives. *Lancet* 382: 260–272, 2013. doi:10.1016/S0140-6736(13)60687-X.
19. **John SG, Sigrist MK, Taal MW, McIntyre CW.** Natural history of skeletal muscle mass changes in chronic kidney disease stage 4 and 5 patients: an observational study. *PLoS One* 8: e65372, 2013. doi:10.1371/journal.pone.0065372.
20. **Kaizu Y, Ohkawa S, Odamaki M, Ikegaya N, Hibi I, Miyaji K, Kumagai H.** Association between inflammatory mediators and muscle mass in long-term hemodialysis patients. *Am J Kidney Dis* 42: 295–302, 2003. doi:10.1016/S0272-6386(03)00654-1.
21. **Koide K, Koshikawa S, Yamane Y, Hidaka S.** Oral adsorbent for therapy of chronic kidney failure. [in Japanese]. *Nihon Rinsho* 49: 758–769, 1991.
22. **Lee SW, Dai G, Hu Z, Wang X, Du J, Mitch WE.** Regulation of muscle protein degradation: coordinated control of apoptotic and ubiquitin-proteasome systems by phosphatidylinositol 3 kinase. *J Am Soc Nephrol* 15: 1537–1545, 2004. doi:10.1097/01.ASN.0000127211.86206.E1.
23. **Lekawanvijit S, Kompa AR, Krum H.** Protein-bound uremic toxins: a long overlooked culprit in cardiorenal syndrome. *Am J Physiol Renal Physiol* 311: F52–F62, 2016. doi:10.1152/ajprenal.00348.2015.
24. **Murphy D, McCulloch CE, Lin F, Banerjee T, Bragg-Gresham JL, Eberhardt MS, Morgenstern H, Pavkov ME, Saran R, Powe NR, Hsu CY; Centers for Disease Control and Prevention Chronic Kidney Disease Surveillance Team.** Trends in prevalence of chronic kidney disease in the United States. *Ann Intern Med* 165: 473–481, 2016. doi:10.7326/M16-0273.
25. **Mutsaers HA, Wilmer MJ, Reijnders D, Jansen J, van den Broek PH, Forkink M, Schepers E, Glorieux G, Vanholder R, van den Heuvel LP, Hoenderop JG, Masereeuw R.** Uremic toxins inhibit renal metabolic capacity through interference with glucuronidation and mitochondrial respiration. *Biochim Biophys Acta* 1832: 142–150, 2013. doi:10.1016/j.bbadis.2012.09.006.
26. **Nishikawa M, Ishimori N, Takada S, Saito A, Kadoguchi T, Furihata T, Fukushima A, Matsushima S, Yokota T, Kinugawa S, Tsutsui H.** AST-120 ameliorates lowered exercise capacity and mitochondrial biogenesis in the skeletal muscle from mice with chronic kidney disease via reducing oxidative stress. *Nephrol Dial Transplant* 30: 934–942, 2015. doi:10.1093/ndt/gfv103.
27. **Peng H, Cao J, Yu R, Danesh F, Wang Y, Mitch WE, Xu J, Hu Z.** CKD stimulates muscle protein loss via rho-associated protein kinase 1 activation. *J Am Soc Nephrol* 27: 509–519, 2016. doi:10.1681/ASN.2014121208.
28. **Picard M, Taivassalo T, Ritchie D, Wright KJ, Thomas MM, Romestaing C, Hepple RT.** Mitochondrial structure and function are disrupted by standard isolation methods. *PLoS One* 6: e18317, 2011. doi:10.1371/journal.pone.0018317.
29. **Piroddi M, Bartolini D, Ciffolilli S, Galli F.** Nondialyzable uremic toxins. *Blood Purif* 35, *Suppl* 2: 30–41, 2013. doi:10.1159/000350846.
30. **Powers SK, Morton AB, Ahn B, Smuder AJ.** Redox control of skeletal muscle atrophy. *Free Radic Biol Med* 98: 208–217, 2016. doi:10.1016/j.freeradbiomed.2016.02.021.
31. **Rao M, Jaber BL, Balakrishnan VS.** Chronic kidney disease and acquired mitochondrial myopathy. *Curr Opin Nephrol Hypertens* 27: 113–120, 2018. doi:10.1097/MNH.0000000000000393.
32. **Romanello V, Sandri M.** Mitochondrial quality control and muscle mass maintenance. *Front Physiol* 6: 422, 2016. doi:10.3389/fphys.2015.00422.
33. **Roshanravan B, Kestenbaum B, Gamboa J, Jubrias SA, Ayers E, Curtin L, Himmelfarb J, de Boer IH, Conley KE.** CKD and muscle mitochondrial energetics. *Am J Kidney Dis* 68: 658–659, 2016. doi:10.1053/j.ajkd.2016.05.011.
34. **Ryan TE, Schmidt CA, Alleman RJ, Tsang AM, Green TD, Neufer PD, Brown DA, McClung JM.** Mitochondrial therapy improves limb perfusion and myopathy following hindlimb ischemia. *J Mol Cell Cardiol* 97: 191–196, 2016. doi:10.1016/j.yjmcc.2016.05.015.
35. **Ryan TE, Schmidt CA, Green TD, Spangenburg EE, Neufer PD, McClung JM.** Targeted expression of catalase to mitochondria protects against ischemic myopathy in high-fat diet-fed mice. *Diabetes* 65: 2553–2568, 2016. doi:10.2337/db16-0387.
36. **Ryan TE, Yamaguchi DJ, Schmidt CA, Zeczycki TN, Shaikh SR, Brophy P, Green TD, Tarpey MD, Karnekar R, Goldberg EJ, Sparagna GC, Torres MJ, Annex BH, Neufer PD, Spangenburg EE, McClung JM.** Extensive skeletal muscle cell mitochondriopathy distinguishes critical limb ischemia patients from claudicants. *JCI Insight* 3: 123235, 2018. doi:10.1172/jci.insight.123235.
37. **Sato E, Mori T, Mishima E, Suzuki A, Sugawara S, Kurasawa N, Saigusa D, Miura D, Morikawa-Ichinose T, Saito R, Oba-Yabana I, Oe Y, Kisu K, Naganuma E, Koizumi K, Mokudai T, Niwano Y, Kudo T, Suzuki C, Takahashi N, Sato H, Abe T, Niwa T, Ito S.** Metabolic alterations by indoxyl sulfate in skeletal muscle induce uremic sarcopenia in chronic kidney disease. *Sci Rep* 6: 36618, 2016. doi:10.1038/srep36618.
38. **Su Z, Klein JD, Du J, Franch HA, Zhang L, Hassounah F, Hudson MB, Wang XH.** Chronic kidney disease induces autophagy leading to dysfunction of mitochondria in skeletal muscle. *Am J Physiol Renal Physiol* 312: F1128–F1140, 2017. doi:10.1152/ajprenal.00600.2016.
39. **Thomas SS, Mitch WE.** Mechanisms stimulating muscle wasting in chronic kidney disease: the roles of the ubiquitin-proteasome system and myostatin. *Clin Exp Nephrol* 17: 174–182, 2013. doi:10.1007/s10157-012-0729-9.
40. **Vanholder R, De Smet R, Glorieux G, Argilés A, Baurmeister U, Brunet P, Clark W, Cohen G, De Deyn PP, Deppisch R, Descamps-Latscha B, Henle T, Jörres A, Lemke HD, Massy ZA, Passlick-Deetjen J, Rodriguez M, Stegmayr B, Stenvinkel P, Tetta C, Wanner C, Zidek W; European Uremic Toxin Work Group (EUTox).** Review on uremic toxins: classification, concentration, and interindividual variability. *Kidney Int* 63: 1934–1943, 2003. doi:10.1046/j.1523-1755.2003.00924.x.
41. **Vanholder R, Glorieux G, De Smet R, Lameire N; European Uremic Toxin Work Group.** New insights in uremic toxins. *Kidney Int* 63: 1934–1943, 2003. doi:10.1046/j.1523-1755.2003.00924.x.
42. **Velenosi TJ, Hennop A, Feere DA, Tieu A, Kucey AS, Kyriacou P, McCuaig LE, Nevison SE, Kerr MA, Urquhart BL.** Untargeted plasma and tissue metabolomics in rats with chronic kidney disease given AST-120. *Sci Rep* 6: 22526, 2016. doi:10.1038/srep22526.
43. **Verzola D, Bonanni A, Sofia A, Montecucco F, D'Amato E, Cademartori V, Parodi EL, Viazzi F, Venturelli C, Brunori G, Garibotto G.** Toll-like receptor 4 signalling mediates inflammation in skeletal muscle of patients with chronic kidney disease. *J Cachexia Sarcopenia Muscle* 8: 131–144, 2017. doi:10.1002/jcsm.12129.

44. **Wang XH, Mitch WE.** Mechanisms of muscle wasting in chronic kidney disease. *Nat Rev Nephrol* 10: 504–516, 2014. doi:10.1038/nrneph.2014.112.
45. **Wang XH, Zhang L, Mitch WE, LeDoux JM, Hu J, Du J.** Caspase-3 cleaves specific 19 S proteasome subunits in skeletal muscle stimulating proteasome activity. *J Biol Chem* 285: 21249–21257, 2010. doi:10.1074/jbc.M109.041707.
46. **Yazdi PG, Moradi H, Yang JY, Wang PH, Vaziri ND.** Skeletal muscle mitochondrial depletion and dysfunction in chronic kidney disease. *Int J Clin Exp Med* 6: 532–539, 2013.
47. **Yokoi H, Yanagita M.** Decrease of muscle volume in chronic kidney disease: the role of mitochondria in skeletal muscle. *Kidney Int* 85: 1258–1260, 2014. doi:10.1038/ki.2013.539.
48. **Zhang L, Rajan V, Lin E, Hu Z, Han HQ, Zhou X, Song Y, Min H, Wang X, Du J, Mitch WE.** Pharmacological inhibition of myostatin suppresses systemic inflammation and muscle atrophy in mice with chronic kidney disease. *FASEB J* 25: 1653–1663, 2011. doi:10.1096/fj.10-176917.
49. **Zhang L, Wang XH, Wang H, Du J, Mitch WE.** Satellite cell dysfunction and impaired IGF-1 signaling cause CKD-induced muscle atrophy. *J Am Soc Nephrol* 21: 419–427, 2010. doi:10.1681/ASN.2009060571.
50. **Zhang YY, Gu LJ, Huang J, Cai MC, Yu HL, Zhang W, Bao JF, Yuan WJ.** CKD autophagy activation and skeletal muscle atrophy-a preliminary study of mitophagy and inflammation. *Eur J Clin Nutr* 73: 950–960, 2019. doi:10.1038/s41430-018-0381-x.